Cellulose (2020) 27:10501–10517
https://doi.org/10.1007/s10570-020-03489-9

ORIGINAL RESEARCH

Electrospun polyacrylonitrile–silica aerogel coating on viscose nonwoven fabric for versatile protection and thermal comfort

M. A. Rahman Bhuiyan · Lijing Wang · Robert A. Shanks · Zinia Anjuman Ara · Tanushree Saha

Received: 16 March 2020 / Accepted: 22 September 2020 / Published online: 7 October 2020

Abstract A novel protective fabric accomplishing with an acceptable level of protective performance and wear comfort has been designed and developed. The protective fabric was tailored by integrating an electrospun PAN–silica aerogel nanofibre membrane with needle-punched viscose nonwoven fabric for simultaneous barrier performance and thermal comfort. The nanofibrous membrane was characterised and evaluated for chemical and thermal protection after sandwiching it within the nonwoven layers. The analysis of PAN–silica aerogel nanofibre revealed that aerogel particles were randomly distributed in the membrane. The nonwoven substrate embedded with the functionalised nanofibre membrane is a lightweight, soft and flexible fabric having versatile protective performance. The newly developed fabric demonstrated satisfactory resistance against radiant heat and liquid chemical penetration. Besides, the improved thermal and moisture vapour transmittance and high evaporative cooling index suggested acceptable thermal comfort of clothing due to the decreased accumulation of perspirations on the material. Moreover, the adequate breathability and moisture management performance indicated diffusion of sweat vapour through the membrane, providing favourable thermal comfort in the clothing-skin microenvironment.

Electronic supplementary material The online version of this article (https://doi.org/10.1007/s10570-020-03489-9) contains supplementary material, which is available to authorized users.

M. A. R. Bhuiyan (✉) · L. Wang · R. A. Shanks · Z. A. Ara · T. Saha
School of Fashion and Textiles, RMIT University, 25 Dawson Street, Melbourne, VIC 3056, Australia
e-mail: s3583256@student.rmit.edu.au

Graphic abstract

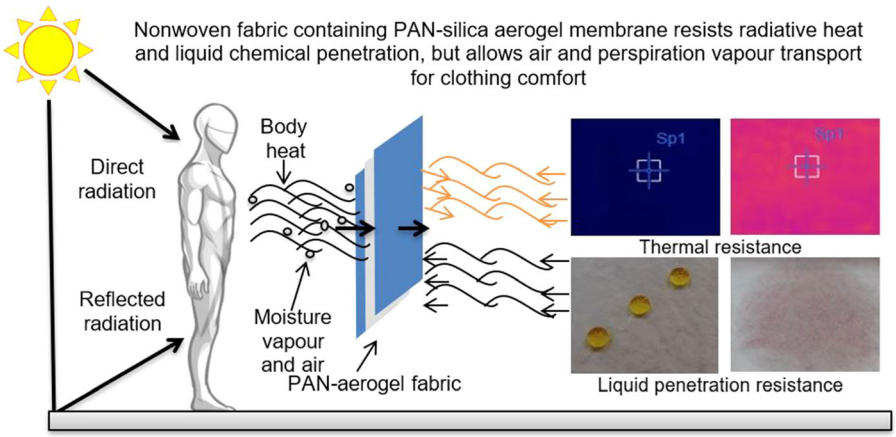

Keywords Protective clothing · Nonwoven fabric · Electrospun nanofibre · Silica aerogel · Chemical protection · Thermal protection · Clothing comfort

Introduction

Protective textiles are fabrics or clothing-related items that are designed to safeguard the wearer from harmful materials along with various environments, and they are considered as the last line of defence under any hazardous conditions (Bhuiyan et al. 2019a). A protective clothing system usually consists of different layers of permeable and impermeable fabric to provide reliable protection (Shaid et al. 2018b), and thus tends to be thick and bulky. Impermeable materials are typically impervious in both directions (Bhuiyan et al. 2019c), causing hyperthermia under hot and humid conditions by inhibiting air and moisture vapour transmission through the fabric (Lee and Kay Obendorf 2006). Therefore, the breathability of clothing is considered as an important factor concerning wearer thermal comfort for working at high temperatures. In this regard, the development of a lightweight, breathable protective clothing system having maximum protection and optimal thermal comfort is essential for such environmental conditions.

Nonwovens are highly porous, permeable fabrics that are commonly fabricated from individual fibrous materials or layers of fibrous webs, rather than yarns (Mao et al. 2007). The fibres in nonwoven fabrics are randomly, directionally oriented and fabricated by several bonding techniques, including thermal, mechanical, and chemical (Wilson 2007). Thus, the construction of nonwovens is distinct from conventional textile structures, such as woven or knitted fabrics. The exceptional structural characteristics of nonwovens lead to excellent thermal-insulating properties by entrapping large volumes of static air in their porous structure (Höffele et al. 2005; Xiong et al. 2018). Hence, the use of nonwoven fabrics in protective clothing systems continues to grow owing to their lightweight and effective thermal protection (Lee and Obendorf 2007).

Nanofibres (NFs) are one-dimensional (1D) ultrathin nanomaterials (Barhoum et al. 2019). Electrospinning is a versatile technique for NF production by solution spinning under an accelerating voltage (Scaffaro and Lopresti 2018). This method is used for creating very fine fibres ranging from less than 100 nm to a few microns (Dhineshbabu et al. 2014). Electrospun fibrous materials possess several interesting features, such as a large surface area to volume ratio, tuneable porosity with interconnected open pore structure, and high permeability (Gavrilenko and Wang 2019; Jahan et al. 2019), making them favourable for use in a wide range of technological applications, including technical textiles. Another notable feature of electrospun nanofibre for use in textiles is the direct application of nanofibrous webs to existing textile materials, such as nonwoven fabrics, for developing protective clothing via coating (Gibson et al. 2001). Since the thickness of electrospun NFs

can be on a submicron scale and with limited strength, any gross movements of such an ultrathin layer on a textile fabric can cause significant damage to the nanofibrous web (Heikkilä et al. 2007). In any barrier clothing having consistent protection, the protective NF layer must be durable with no breaking or delaminating during the movements of the substrate. The use of a nanofibrous membrane between any strong and stable materials can therefore be considered an effective approach by shielding against any external force that might cause the damage to the nanofibre. Thus, a sandwich-like structure having a nanofibrous membrane between two layers of textile fabric substrates is proposed for a durable and adaptable NF layer in a protective clothing system with enhanced functional properties.

Electrospun NFs are generally made of various polymers, including poly(vinyl chloride) (PVC), poly(vinyl alcohol) (PVA), polyacrylonitrile (PAN), poly(vinylidene fluoride) (PVDF), and poly(vinylidene fluoride–co–hexafluoropropylene) (PVDF-HFP) (Yanilmaz et al. 2014). Among these polymers, PAN is the most preferred as a starting material for the fabrication of nanofibrous membranes due to its ease of polymerisation, large specific surface area, and excellent stability against chemicals (Nie et al. 2013; Wang et al. 2014). However, the low thermal stability of the PAN nanofibre membrane prevents its widespread application, especially in high-temperature media (Mao et al. 2012).

Silica aerogel is a lightweight porous material with different pore sizes ranging from 2 to 50 nm (Dorcheh and Abbasi 2008). The nanoporous structure with an extremely high porosity (as high as 99.0%) and ultra-low thermal conductivity ($\sim$ 13 mW/m K) makes silica aerogel an impressive thermal insulating material (Kiil 2015). Thus, modification of PAN NFs using electrospun PAN membrane embedded with inorganic materials such as silica aerogel is of great interest because of their thermal and chemical stability (Li et al. 2003). Additionally, the incorporation of silica particles exhibits a considerable change to the morphology and porous structure of the subsequent nanofibre web by creating a hierarchical roughness on the membrane surfaces (Wang et al. 2014). Silica aerogel has gained attention for extensive applications in textiles for the development of thermal insulative fabric, including spacesuit insulation (Paul and Diller 2003), extreme cold weather clothing (Venkataraman et al. 2015), and thermal liner for fire protective garments (Jin et al. 2013; Shaid et al. 2016). However, a minimal investigation has been directed towards the scope of using silica aerogel in barrier clothing for chemical protection via liquid chemical adsorption by employing its porous structure.

Our earlier studies revealed the prospect of using silica aerogel in chemical protective clothing that has synchronized protective performance and thermal comfort. However, maximum protection with acceptable clothing comfort remains a challenging issue that requires greater attention. Polyurethane (PU)–silica aerogel incorporating a chemical protective coating on cotton fabric (Bhuiyan et al. 2019b) had some limitations, including high stiffness and thickness, along with low air and moisture vapour permeability because of partial or entire filling of the porous fabric structure by the PU binder. Silica aerogel integrated thermal bonded nonwoven fabrics (Bhuiyan et al. 2020) demonstrated simultaneous chemical and thermal protection with adequate air and moisture vapour permeability. However, the high thickness and bulkiness due to the many dusted aerogel particles in the fabric and the thermal bonding of fibres within the fabrics is anticipated to increase the stiffness and reduce the cloth drapability for wear comfort.

In this contribution, we aim to extend our previous investigation by developing a new class of flexible protective clothing via integrating electrospun PAN–silica aerogel nanofibrous membrane, with needle-punched viscose nonwoven fabric for the required level of protection along with acceptable wear comfort. Nanofibrous membrane incorporated with aerogel particles is characterised and evaluated for liquid chemical and heat protection after it is embedded within the nonwoven fabric. An objective is to assess the protective performance concerning thermal and chemical protection by analysing the resistance against radiant heat and liquid penetration. Clothing comfort in terms of fabric softness, dry and evaporative heat transmittance, air permeability, and moisture management property are investigated to assess the potential application of PAN–silica aerogel nanofibrous membrane in a protective clothing system.

Experimental

Materials

Viscose staple fibre having an average length of 38 mm and fineness of 1.5 D (denier) was procured from Tianjin Glory Tang Fiber Technology Co., Ltd, China as the raw material for the nonwoven fabrics. For electrospinning, PAN powder was provided by Goodfellow Cambridge Ltd, UK. Enova silica aerogel (IC3110) was obtained from Cabot Corporation, USA. Typical parameters of both the PAN powder and silica aerogel particles are listed in Table 1.

Liquid organic and inorganic chemicals used to assess the fabric chemical resistance, including methanol, *N*,*N*-dimethylformamide (DMF), and toluene were collected from Chem-Supply Pty Ltd, Australia. Acetone, sodium hydroxide, and sulphuric acid were procured from Sigma Aldrich Pty Ltd., Australia, and acetonitrile was obtained from BDH Chemicals Ltd, England.

Methods

Nonwoven fabric substrate

Viscose is a regenerated cellulosic fibre with excellent hydrophilicity (Mortan and Hearle 2008). Therefore, viscose staple fibre was employed to produce the nonwoven fabric with enhanced moisture/water absorption capability. To manufacture the needle punched nonwoven fabric initially, a dry-laid web was developed by opening and feeding fibres to the carding machine (Shin Chang Industry Co., Ltd, Taiwan) (Fig. S1a). The nonwoven was fabricated by passing the dry-laid web through the needle punching machine (Shoou Shyng Machinery Co., Ltd, Taiwan) (Fig. S1b).

Tailoring nonwoven/PAN–aerogel nanofibre fabric

An 11.0% w/v polymer solution for electrospinning was prepared by dissolving PAN powder into DMF solvent followed by continuous mechanical stirring at room temperature for 24 h. Aerogel particles were ground mechanically using a mortar and pestle, and the size of the particles was reduced to 35–340 μm. Then, silica aerogel microparticles were added to the prepared PAN solution and stirred at the same temperature until homogeneity was achieved. The properties of the pure PAN and PAN–aerogel solution, including viscosity and conductivity were analysed by using a viscometer (Falling ball viscometer, Model KF40, Brookfield Engineering Laboratories Inc., USA) and conductivity metre (Micro 800, Palintest Ltd., Singapore). A maximum 4.0% w/v of aerogel was incorporated into the PAN solution, which has the required viscosity suitable for the development of electrospun jet during the processing. Besides, an intermediate concentration of PAN–aerogel (2.0% w/v) was used to evaluate the effect of silica aerogel particles in the membrane. Solutions comprising of pure PAN and PAN–aerogel of different concentrations were electrospun on the surface of nonwoven material to fabricate the PAN and PAN–aerogel hybrid functional nanofibrous membrane. The equipment configuration used to produce the PAN and PAN–aerogel nanofibrous layer on viscose nonwoven fabric is described in Table 2.

The nonwoven fabric (32 cm × 32 cm) attached with the electrospun nanofibre membrane of pure PAN or PAN–aerogel was covered with another layer of nonwoven of similar thickness followed by heat setting at the edge of fabrics using a fusible interlining. Heat setting was performed at 140 °C and a pressure of 6.0 kPa for 3 min. The fabrication of nonwoven–PAN and nonwoven–PAN–aerogel fabric is presented schematically in Fig. 1.

Table 1 The characteristic parameters of silica aerogel and PAN powder

Silica aerogel		PAN powder	
Parameter	Physical property	Parameter	Physical property
Physical state	Solid	Physical state	Solid
Form	Powder	Form	Powder
Particle size	100–700 μm	Particle size	50 μm
Particle density	120–150 g cm^{-3}	Bulk density	0.34–0.39 g cm^{-3}
Pore diameter	~ 20 nm	Molecular weight	85,000 g/mol
Surface chemistry	Hydrophobic	Colour	White

Table 2 Laboratory equipment arrangement for the pure PAN and PAN–aerogel nanofibrous membrane

Parameters	Specifications
Electrode distance	120 mm
Flow rate	0.75 mL h^{-1}
Voltage	15 kV
Needle size (inner diameter)	0.84 mm
Collector drum speed	10 rpm

model 11430, USA). Energy-dispersive X-ray (EDX) analysis was conducted by employing FEI Quanta 200 ESEM and Aztec software. The specimens were prepared by coating with carbon (10 nm thickness) using a Gatan precision etching and coating system (Model 682, PECS, USA). The spots were selected randomly for map scanning of each specimen, and the average spectra were presented. An FTIR spectrometer (PerkinElmer Spectrum 400 FTIR, USA) was employed to examine the existence of silica aerogel

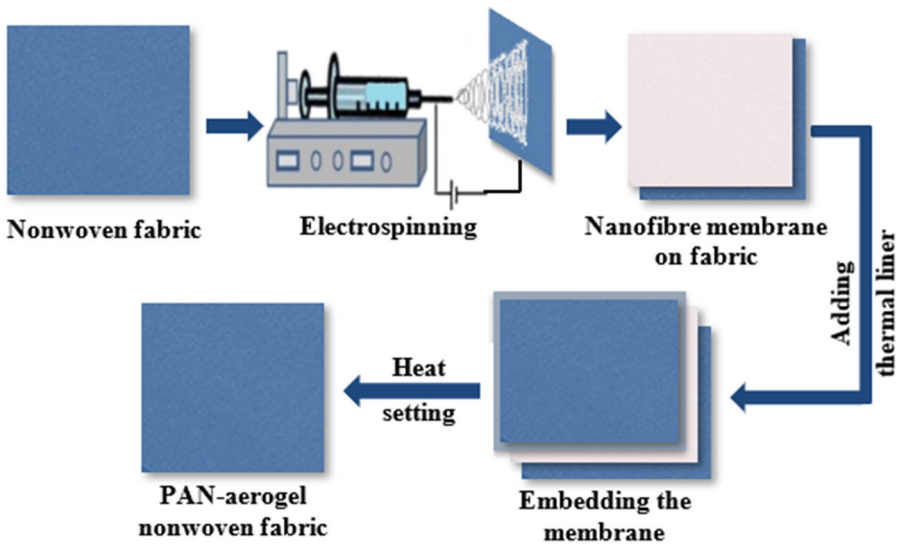

Fig. 1 Schematics of producing nonwoven–PAN and nonwoven–PAN–silica aerogel fabric

The control nonwoven fabric (without electrospun membrane) was prepared by attaching two nonwoven fabric layers via heat setting, as mentioned above. Then the control nonwoven, pure PAN, and PAN–aerogel hybrid nonwoven fabrics were coded respectively as CF, PF, PAF1 (2.0% w/v), and PAF2 (4.0% w/v) for further studies.

Characterisation and evaluation

Morphological analysis

The morphological investigation of the nanofibrous membrane was conducted by using scanning electron microscopy (FEI Quanta 200 ESEM), a low vacuum mode with 20 kV accelerating voltage. Before the SEM analysis, the specimens were coated with Au for 60 s using a sputter coater (SPI Sputter Coating Unit, particles in the nanofibre matrix. The experiment was conducted in transmission mode over the spectral range of 4000–400 cm^{-1}, with 16 scans averaged for each spectrum.

Fabric physical properties

The weight of the fabric in terms of mass per unit area (g m^{-2}) was measured according to ASTM D3776–96 standard. The test of fabric thickness was conducted using a fabric thickness tester following the method ASTM D1777–15. Fabric stiffness was measured as per the ASTM D1388–08 standard by using the Shirley stiffness tester, from Shirley Development Ltd., England. During the test, each fabric specimen was cut to a size of 250 mm × 25 mm using a template. Then the stiffness in terms of flexural rigidity was determined by using Eq. 1 after

measuring the bending length (bending of the fabric under its own mass to an angle of 41.5°) of fabric.

$$G = 9.8mC^3 \times 10^{-6} \quad (1)$$

where G is the flexural rigidity (μN m), C is the mean bending length (mm), and m is the mass per unit area of the cloth (g m^{-2}).

Resistance to chemical penetration

The chemical penetration resistance of fabrics was determined according to the BS ISO 22608:2004 method. The test was conducted by using water and different organic and inorganic liquid chemicals, as mentioned in the ASTM F1001-12 standard. The liquid resistance was assessed in terms of repellency, retention, and penetration of chemicals through the fabric. During the experiment, liquid chemicals (0.2 mL) were dropped onto the fabric surface after placing the specimen (8 cm × 8 cm) on a flat, smooth surface. The fractions of repellency, retention, and penetration of the test liquid through the fabric specimens were calculated from Eqs. 2, 3, and 4, respectively.

$$Repellency = m_a/m_t \times 100 \quad (2)$$

$$Retention = m_b/m_t \times 100 \quad (3)$$

$$Penetration = m_c/m_t \times 100 \quad (4)$$

where m_t is the total mass of chemical (mg) released on the fabric, m_a is the mass of liquid (mg) removed from the fabric surface, m_b is the mass of liquid (mg) retained by the specimen and m_c is the mass of liquid (mg) penetrated through the fabric.

Radiant heat resistance

The radiative heat resistance regarding the thermal protection of clothing was evaluated by employing a bench-scale test instrument. This apparatus was developed by Shaid et al. (2019), and the detailed test procedure was also mentioned therein. The heat resistance was measured after exposing the fabrics on a hot plate of 250 °C and subjected to radiant heat, maintaining a constant distance of 15 cm. The increase of temperature beneath the exposed fabric was determined by heat sensors and recorded every two seconds. The test was terminated when the fabric temperature reached 55 °C (i.e., second-degree burn temperature). The time required to reach 44 °C (i.e., pain threshold) and 55 °C were recorded from the time-temperature readings. Accordingly, the mean value was reported after repeating the test at least three times for each fabric.

The thermal resistance of fabrics was also evaluated by thermal imaging of the specimens using a thermographic infrared camera (FLIR T400-series). The images were taken after placing the fabric on a uniform hot surface with a constant temperature of 100 °C. Then the imaging was performed over 60 s at 100 cm from the top of the fabric, and the maximum and minimum temperature of each specimen was recorded from that period.

Thermal and evaporative resistance and air permeability

The thermal and evaporative resistance of test fabric specimens was determined following the standard ISO 11092:2014 by using an Integrated Sweating Hotplate (Model 431-213). The standard atmospheric conditions of the test chamber for both the experimental investigations are shown in Table 3.

Table 3 Standard atmospheric conditions for fabric thermal and evaporative heat resistance testing

Test condition	Thermal	Evaporative
Relative humidity	65.0 ± 3.0%	40.0 ± 3.0%
Air velocity	1.00 ± 0.05 m/s	1.00 ± 0.05 m/s
Air temperature	20.0 ± 0.1 °C	35.0 ± 0.1 °C
Thermal guard	35.0 ± 0.1 °C	35.0 ± 0.1 °C

The actual dry heat resistance (at the steady-state condition of the system) provided by the fabric alone was calculated according to Eq. 5.

$$R_{cf} = R_{ct} - R_{cb} = \frac{(T_s - T_a)}{Q/A} - R_{cb} \quad (5)$$

where R_{cf} = fabric thermal resistance (m^2 °C/W); R_{ct} = total thermal resistance provided by the fabric and air layer (m^2 °C/W); R_{cb} = bare plate resistance (m^2 °C/W); T_s = average temperature of plate surface (°C); T_a = air temperature (°C) and Q/A = area weighted heat flux (W/m^2).

The actual fabric evaporative heat resistance was determined using Eq. 6.

$$R_{ef} = R_{et} - R_{eb} = \frac{(P_s - P_a)}{Q/A} - R_{eb} \quad (6)$$

where R_{ef} = fabric evaporative resistance (P_a m^2/W); R_{eb} = bare plate resistance (P_a m^2/W); R_{et} = total evaporative resistance provided by the fabric system, liquid barrier and air layer (P_a m^2/W); P_s = saturation vapour pressure at the plate surface temperature (Pa); P_a = vapour pressure at air temperature (Pa) and Q/A = area weighted heat flux (W/m^2).

Besides, the moisture permeability index (i_{mt}) of fabric was determined from the average value of thermal and evaporative transmittance of each fabric using Eq. 7.

$$i_{mt} = K\left(\frac{R_{ct}}{R_{et}}\right) \quad (7)$$

where K is a constant (60.6515 Pa/°C).

The air permeability was determined according to ISO 9237:1995 using an air permeability tester (M021S, SDL Atlas Pty Ltd, England). The test was conducted at a pressure of 100 Pa using a 5.0 cm^2 working area of fabric. Then mean air permeability (mL cm^{-2} s^{-1}) was calculated and presented from eleven air flow readings for each fabric.

Moisture management property

The moisture management performance of fabric specimens was assessed by following the standard AATCC-TM-195-2010. The experiment was conducted after placing the specimen (80 mm × 80 mm) between the top and bottom sensors in the test chamber of the machine (M 290, SDL Atlas Ltd). A predetermined amount of standard test solution (9.0 g L^{-1} NaCl) as sweat was dropped onto the top surface of the fabric (i.e., the skin or inner side of the apparel) for 20 s and the absorption of the liquid from the inner to outer surfaces was observed for 120 s.

The conditioning of all fabric specimens was performed in controlled atmospheric condition (20 ± 2 °C temperature and 65 ± 3% RH, except for the evaporative test at 35 ± 2 °C temperature and 40 ± 3% RH) for at least 24 h in the laboratory, followed by the respective standard before experimenting in the same environment.

Results and discussion

Material characterisation

Morphological analysis

The surface morphology of the pure PAN membrane in Fig. 2a shows a three dimensional (3D) fibrous structure and randomly oriented regular PAN NFs in the membrane. However, the PAN–aerogel (4.0%) membrane in Fig. 2b exhibited randomly deposited aerogel particles that were well scattered in the matrix of the membrane. The SEM image of the PAN–aerogel NFs also revealed a larger size of aerogel particles in the membrane that were grounded mechanically before adding to the spinning solution. This might be due to the deposition of aerogel particles in the aggregated form during the electrospinning. Besides, the bunching of aerogel particles on a certain number of NFs was detected in Fig. 2b. The EDX spectrum of PAN–aerogel NFs further confirmed the presence of silica in the membrane (Fig. 2c), and their random distribution throughout the membrane was explored by the EDX area mapping image of the surface (Fig. S2b).

The EDX spectroscopy was validated by comparing the FTIR spectra of pure PAN and the PAN–silica aerogel NFs composite in Fig. 2d. The characteristic Si–O–Si vibrational mode peak at 1066 cm^{-1} (high-intensity peak) (Kapridaki and Maravelaki-Kalaitzaki 2013) and typical bending mode peaks at 843 and 780 cm^{-1} (Ji and Zhang 2008) for the PAN–silica NFs confirm the existence of aerogel particles in the membrane. On the other hand, the spectrum of pure PAN NFs (Fig. 2d) contains a prominent peak at 2243 cm^{-1} due to the stretching vibration of nitrile groups (–CN–) (Zhang et al. 2007). The peaks at 2930 cm^{-1} and 1470 cm^{-1} belong to the methylene ($–CH_2–$) group stretching and bending vibrations, respectively (Wu et al. 2012). The stretching vibration of the carbonyl peak (> C = O) at 1731 cm^{-1} was associated with the PAN NFs deposited from the DMF solution (Ji and Zhang 2008).

A considerable increase in fibre diameter of PAN–aerogel NFs (PAF2: 259.1 ± 14.7 nm) compared with the pure PAN NFs (PF: 199.8 ± 9.6 nm) was revealed from the morphological investigation (Fig. S3c, d). This was attributed to the increased viscosity, along with the decreased conductivity of the resultant solutions after the integration of aerogel particles (Babar et al. 2017).

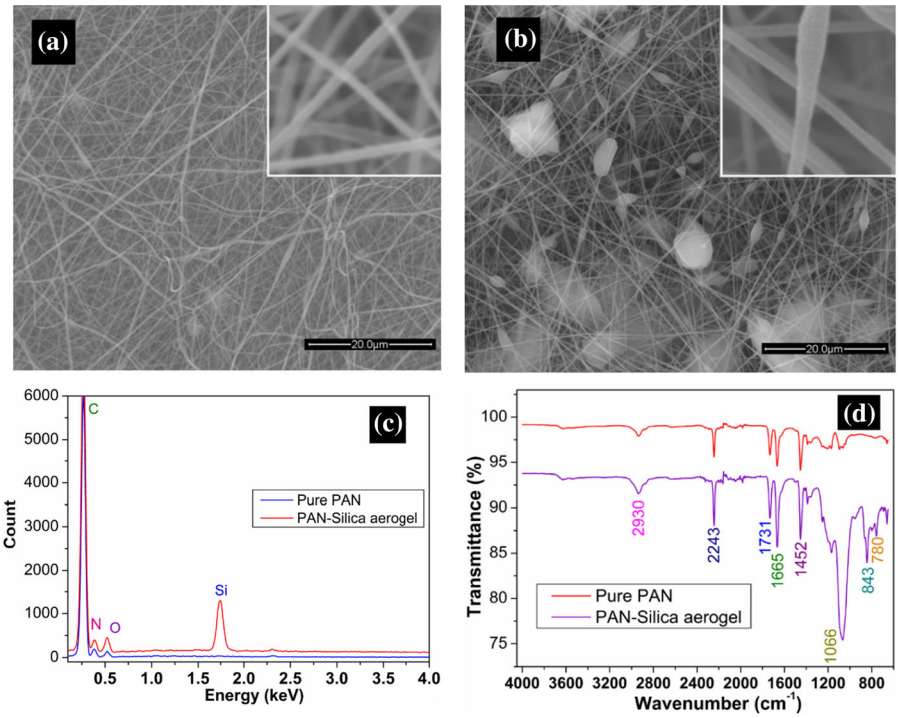

Fig. 2 SEM micrographs of **a** pure PAN nanofibres and **b** PAN–silica aerogel (4.0%) nanofibres, **c** EDX and **d** FTIR spectra of pure PAN (PF) and PAN–silica aerogel nanofibre of 4.0% aerogel content (PAF2)

The viscosity of the pure PAN solution was 533.4 mPa s, whereas after the addition of 4.0% aerogel, it was increased to 3103.7 mPa s (Table S1). Because of high viscosity, the electric field could not draw the electrospun jet equivalently at the same applied voltage during processing (Ghaffari et al. 2019), which resulted in thicker nanofibers for higher concentration. This morphological change of the PAN–aerogel NFs leads to increased porosity or less surface covering of the membrane (Fig. S3a, b), due to the formation of less thick NFs from the same volume of solution. Accordingly, the nonwoven fabric integrated with a porous nanofibrous membrane is anticipated to allow the transfer of air and perspiration vapour that will provide improved breathability for satisfactory thermal comfort.

Fabric physical properties

The physical properties of the newly developed protective fabric, including the thickness, weight, and stiffness were measured. No significant differences in thickness was observed among the fabrics, as shown in Fig. 3a. This was due to the tailoring of the specimens from the nonwoven layers having nearly the same thickness and weight. The control nonwoven specimen had the minimum thickness, and a slight increase was observed after integrating the nanofibrous membrane. Accordingly, all fabric specimens exhibited a slight increase in mass per unit area (Fig. 3a). Although a maximum average weight of 178 g m^{-2} was noticed for the PAN–aerogel fabric (PAF2) having an aerogel concentration of 4.0%; however, this weight is still significantly lower compared with the various commercial protective fabrics (400–600 g m^{-2}) mentioned in current studies (Bhuiyan et al. 2020; Shaid et al. 2018b).

Nonwoven fabrics are porous due to the structural feature of fibrous webs or individual fibres. Because of the structural porousness, the thickness of nonwovens increased considerably without much influencing their

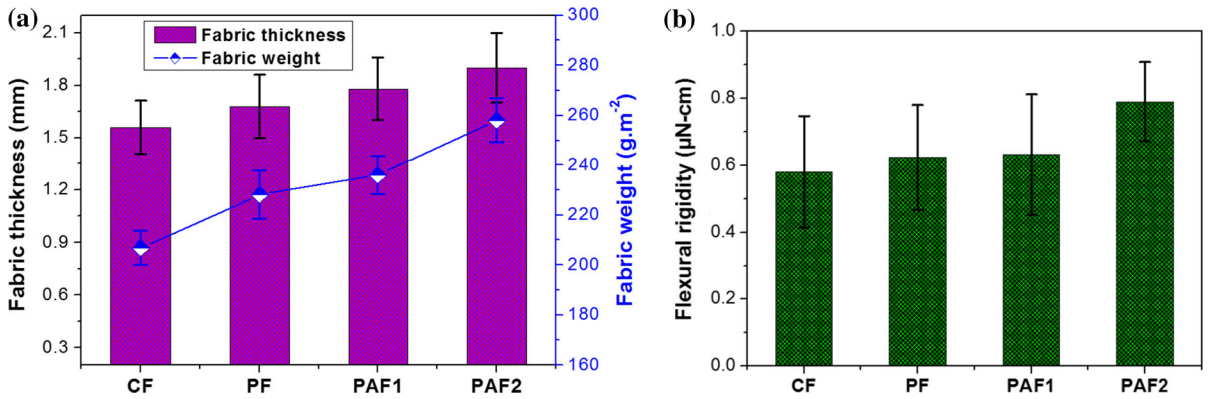

Fig. 3 Change of fabric physical parameters **a** thickness and weight, **b** flexural rigidity before and after integration of nanofibrous membrane

mass per unit area; and therefore, the fabrics were much lighter compared with woven fabrics of similar thickness. Moreover, the characteristic nonuniformity of nonwovens in either thickness and weight or in both (Mao et al. 2007) leads to a greater standard deviation (SD), as explored in Fig. 3a.

The flexural rigidity concerning stiffness of the experimental fabrics is presented in Fig. 3b. Fabric stiffness is the bending of cloth in one plane under its weight, and this term is commonly used for the subjective assessment of clothing quality relating to the handle or drape of the fabric. The control nonwoven fabric showed the lowest flexural rigidity; therefore, it has the least resistance against bending corresponding to maximum drapability. A slight increase in flexural rigidity was noticed for the fabrics integrated with the PAN–aerogel membrane. However, the changes of stiffness were not significant compared with the control nonwoven fabric, and the trivial changes suggest a slight or minimal effect of nanofibrous membrane on the flexibility of the fabric. This unchanged fabric flexibility with a low weight of the fabric can be employed to fabricate lightweight drapable protective clothing for providing physiological wear comfort to the user.

Protective performance

Chemical protection

The chemical protection concerning the resistance against liquid chemical penetration through the fabric is shown in Fig. 4. Chemical resistance was assessed by determining the fractions of repellency, retention, and penetration of liquids through the fabric. As viscose is a hydrophilic fibre with excellent liquid absorption capacity, the chemicals were absorbed rapidly when coming in contact with the surface of viscose fabric. Thus, all the test nonwoven fabrics demonstrated a zero (0%) repellency against the liquid chemicals, and most of the chemicals were absorbed into the fabric (Fig. 4a). Hence, the chemical resistance exhibited by the nonwovens was only through the retention of liquids into the fabric with no spreading on the fabric surface.

Figure 4b shows that the control fabric has the least resistance against chemical penetration, and all the liquids were penetrated through the fabric, following an initial absorption process. Due to absorption, some fractions of the liquid were retained in the fabric. The highest retention was observed for chemicals with low volatility, including sodium hydroxide solution (50.0%) and water (Fig. 4a). Some chemicals were evaporated as the evaporation loss during the experiment, and the highly volatile liquids lead to a maximum loss of evaporation. Therefore, minimum retention and penetration were noticed for those chemicals, as shown in Fig. 4. Besides, the maximum penetration of H_2SO_4 (93.1%) in the case of control nonwoven fabric was due to the dissolving of viscose fibres in the concentrated acid solution, which was penetrated rapidly through the specimens without much retaining in the fabric.

Improved chemical resistance was observed after sandwiching the nanofibrous membrane inside the nonwoven fabric. The hydrophobicity of the PAN NF

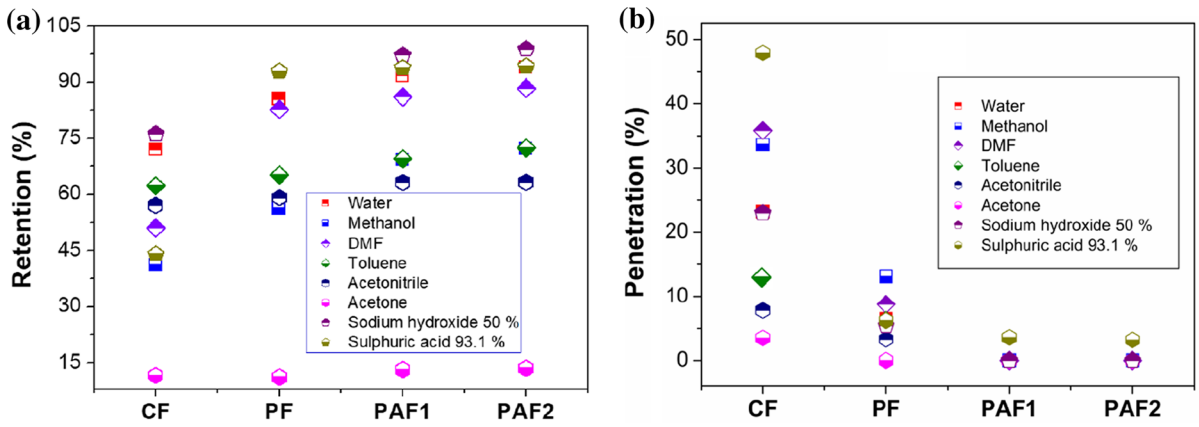

Fig. 4 Liquid penetration resistance of fabric **a** retention and **b** penetration of liquids through the fabric

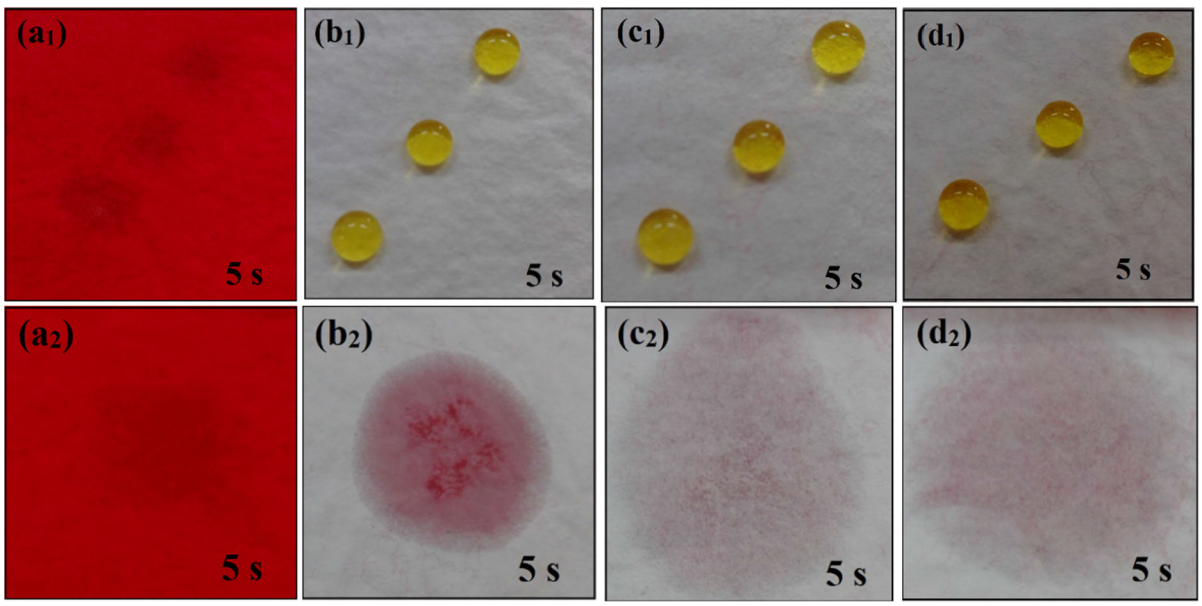

Fig. 5 Exposing of the chemical resistance mechanism after removing the top layer fabric-control fabric, PAN–nonwoven, PAN–aerogel nonwoven (2.0%), and PAN–aerogel nonwoven (4.0%) fabrics, respectively against the chemicals of $\mathbf{a_1}$, $\mathbf{b_1}$, $\mathbf{c_1}$, $\mathbf{d_1}$ high surface tension (sodium hydroxide solution 50.0% w/v:101.0 dyne cm^{-1}) and $\mathbf{a_2}$, $\mathbf{b_2}$, $\mathbf{c_2}$, $\mathbf{d_2}$ low surface tension (methanol: 22.7 dyne cm^{-1})

membrane (Im et al. 2008), along with its less porosity, provided some resistance against the flowing of liquids through the fabric. Therefore, the fabric PF exhibited a higher liquid penetration resistance than the control specimens but inferior to the PAN–aerogel specimens (Fig. 4b). The penetration resistance increased significantly after incorporating the porous silica aerogel particles in the nanofibrous membrane. Thus, the fabrics PAF1 and PAF2 exhibited the maximum chemical resistance with no penetration (except for a concentrated H_2SO_4 solution where viscose fibres dissolved rapidly and created scope for slight penetration of liquids through the membrane) of liquids through the fabric (Fig. 4b).

Silica aerogel is an extremely hydrophobic material with exceptional porosity, hence, the embedding of aerogels with the hydrophobic PAN nanofibre might enhance the overall hydrophobicity of the membrane

to resist the penetration of chemicals with high surface tension (Fig. 5b_1, c_1, d_1). In the case of liquids with a low surface tension, the chemicals were absorbed initially by the fibre on the fabric surface following the adsorption through the pores of aerogel particles embedded within the membrane (Fig. 5c_2, d_2). The wide-ranging of silica aerogel pore sizes (5–100 nm), as well as their open pore network due to interconnectivity with each other, enabled the adsorption of liquids by flowing the chemicals from one pore to another with limited restriction (Bhuiyan et al. 2019b). Accordingly, liquid chemicals became spread out on the membrane surface without penetrating through the nanofibre because of adsorption by the aerogel particles. The presence of more aerogel particles enhanced the overall liquid adsorption. The more liquid adsorption will create scope to retain a greater amount of chemicals in the fabric, and consequently, the more reliable protection against the liquid chemical penetration can be achieved.

Thermal protection

The fabric thermal protection performance was assessed by determining the resistance against radiant heat. The comparative performance was analysed from the time-temperature curves (Fig. 6a) after exposing the fabrics to a heat source of 250 °C. Raising the temperature to 55 °C beneath the exposed fabric was the endpoint of the experiment. Because human skin receives an irreversible second-degree burn when the skin temperature approaches at 55 °C (Shaid et al. 2018a). Besides, the pain threshold, i.e., the temperature at which skin starts to feel pain (44 °C) and first-degree burn temperature (48 °C) (Shaid et al. 2018b) were determined from the time–temperature curves. The escape time, time for withdrawing from the danger of burning, is another important parameter for thermal protection. It was calculated from the time gap between the pain threshold (44 °C) and second-degree burn temperature (55 °C) (Bhuiyan et al. 2020). The resistance of fabrics against radiative heat was assessed by comparing and analysing the time to reach the pain threshold and receiving second-degree burn temperature.

Figure 6a illustrates the rise in fabric temperature after exposure to a radiant heat source. Control nonwoven specimens (CF) demonstrated the least resistance among the fabrics and reached the pain threshold and the first-degree burn temperature within 296 s and 378 s of heat exposure, respectively. The heat resistance increased significantly for the fabrics embedded with the nanofibrous membrane. Therefore, PAN–nonwoven fabrics (PF) showed better resistance (425 s and 540 s to reach 44 °C and 48 °C, respectively) compared with the control specimen, but were inferior to the PAN–aerogel specimens. The PAN–aerogel (4.0%) nonwoven fabric (PAF2) exhibited the greatest resistance against the radiant heat, and a maximum time 490 s and 618 s were recorded to reach the pain threshold and first-degree burn temperature, respectively. Likewise, PAF2 showed the longest time (960 s) to reach the irreversible second-degree burn temperature (Fig. 6b), as well as the

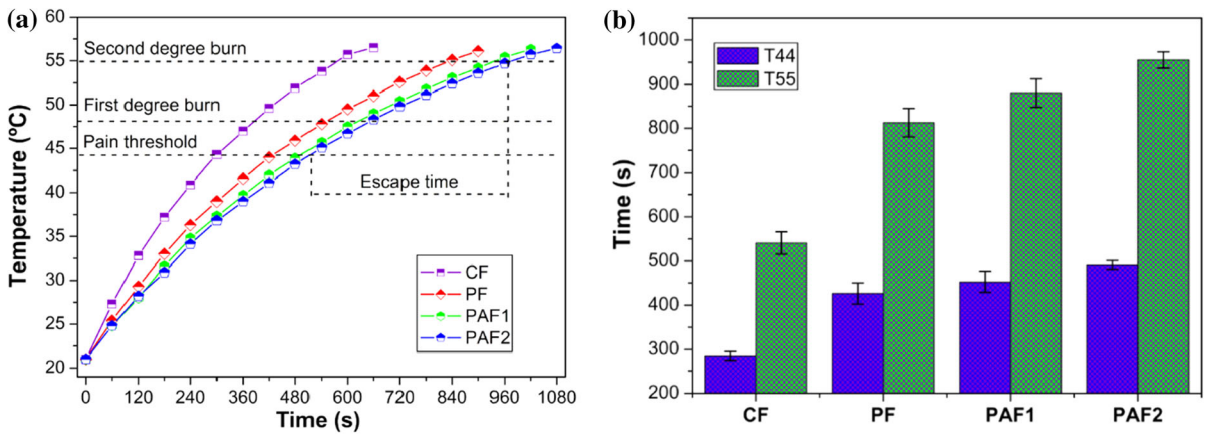

Fig. 6 Thermal protection of fabrics. **a** Comparative radiant heat resistance performance **b** time required to reach pain threshold (T_{44}) and irreversible second-degree burn temperature (T_{55}). Data are represented as mean ± standard deviation (SD)

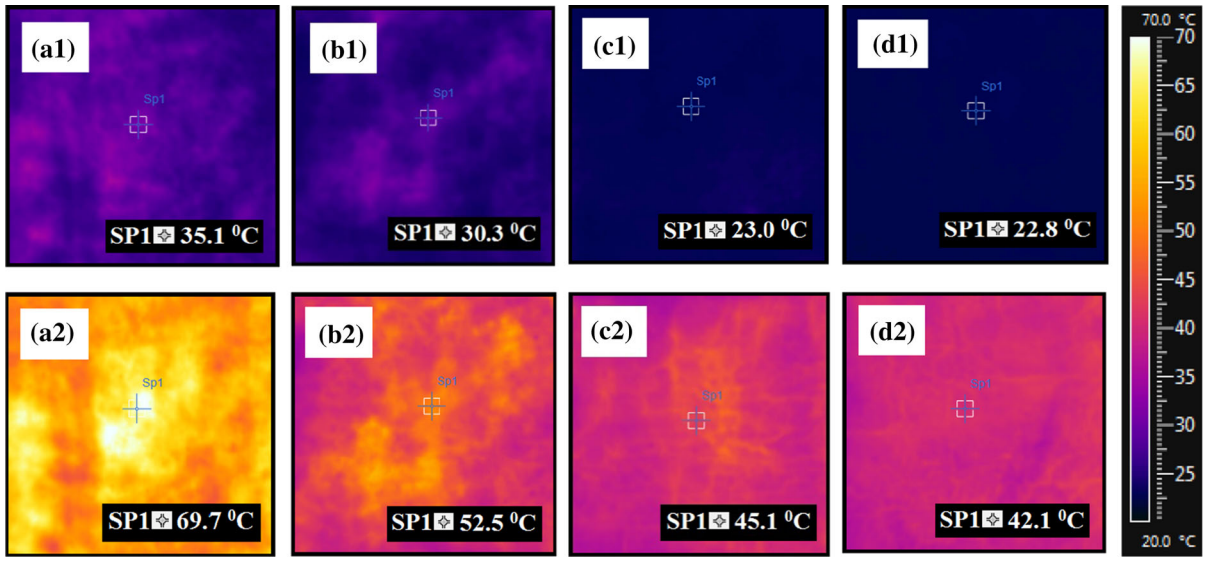

Fig. 7 IR thermography images of **a** control fabric, **b** PAN–nonwoven, **c** PAN–aerogel nonwoven (2.0%), and **d** PAN–aerogel nonwoven (4.0%) fabrics at 5 s ($\mathbf{a_1}$, $\mathbf{b_1}$, $\mathbf{c_1}$, $\mathbf{d_1}$) and 60 s ($\mathbf{a_2}$, $\mathbf{b_2}$, $\mathbf{c_2}$, $\mathbf{d_2}$)

maximum escape time (460 s) among all the specimens.

The thermal resistance of nonwoven fabrics in contact with the hot surface (100 °C) was evaluated by thermography images using an infrared thermal camera. The increase in fabric surface temperature because of heat was recorded over 60 s, and the thermal images of fabric at 5 s and 60 s is shown in Fig. 7. An abrupt increase in temperature with time was noticed for the control fabrics (Fig. S4) with the temperatures of 36.1 °C and 67.3 °C at 5 s and 60 s, respectively (Fig. 7a_1, a_2). The rise in temperature slowed down after embedding the nanofibrous membrane as well as the increase of aerogel concentration in the membrane. Thus, the PAN–aerogel (4.0%) nonwoven fabric (PAF2) exhibited the least increase in temperature within 60 s of heat exposure (Fig. 7d_1, d_2), suggesting the greatest thermal resistance among the fabrics.

Heat resistance of textiles is closely connected with the construction and density of the fabric, as well as the thermal resistance of constituent fibres (Houshyar et al. 2015). As discussed earlier, the nonwoven structure possesses an exceptional porosity, and therefore provided an excellent thermal resistance by entrapping large volumes of still air in the porous structure. Besides, the high thickness of nonwoven fabrics compared with weight (Fig. 3), and the low thermal conductivity of viscose fibres (Mortan and Hearle 2008) increased the thermal resistance according to Eq. 8 (Frydrych et al. 2002).

$$R = \frac{\sigma}{\lambda} \tag{8}$$

where R is the thermal resistance, σ is the cloth thickness and λ is the thermal conductivity.

An improvement of fabric thermal resistance after integrating the nonwoven with the nanofibrous membrane was due to the packed structure of the membrane comprised of a high-density NF layer. The nanofibrous membrane with high packing density reduced the mean free path (distance travelled by a photon before it collides with another) for a photon movement, and therefore decreased conduction by hindering the overall heat transfer (Venkataraman et al. 2018). Electrospun NF made of polyacrylonitrile has a positive impact on the thermal insulation of clothing (Ghaffari et al. 2019); thus, a considerable increase in thermal resistance was observed for the PAN–nonwoven fabrics. Besides, the incorporation of silica aerogel with the PAN NF demonstrated the superior thermal resistance. The silica aerogel possesses an excellent thermal insulative property. The high thermal insulation of aerogels suppressed the heat conduction and convection, while the large specific surface area of the nanofibrous membrane decreased the radiative heat transfer by scattering and absorbing

the heat (Sabetzadeh et al. 2012). Accordingly, the PAN–aerogel nonwoven fabric acts as an insulating material, providing satisfactory thermal protection to the wearer by hindering the flow of heat from any external heat source.

Thermal comfort

Thermal and evaporative resistance and air permeability

Thermal and evaporative resistance of fabric indicates its ability to resist the flow of dry and evaporative heat from the body to the atmosphere (Bhuiyan et al. 2019c). The total metabolic body heat, i.e., the sum of dry and perspiration vapour transmittance, is directly related to the thermal comfort of clothing. A fabric with completely dry and evaporative resistance can cause hypothermia under hot and humid environments, and therefore, these two terms are commonly considered as the primary parameters determining apparel thermophysiological wear comfort. Besides, the moisture permeability index or evaporative cooling index (i_{mt}) is another clothing parameter stating the relationship between dry and evaporative resistance in relation to thermal comfort (Bhuiyan et al. 2019b). The moisture permeability index has a theoretical range from 0 to 1, where 0 refers to being completely impermeable, and 1 denotes an ideally permeable fabric (Woodcock 1962).

Figure 8a shows an increase in thermal resistance of fabrics integrated with the NF membrane. A further improvement was noticed for the PAN–aerogel fabric, and the specimen having an aerogel concentration of 4.0% (PAF2) demonstrated the maximum thermal resistance (Fig. 8a). This was due to the structural characteristics of nonwoven fabrics, as well as the presence of silica aerogel particles, as discussed earlier. The nonwoven fabric itself increased thermal resistance by entrapping still air in their porous structure. Besides, the integration of nonwoven fabric with the nanofibrous membrane with low thermal conductive silica aerogel particles contributed to the further increase in thermal resistance.

In the case of evaporative transmittance (R_{ef}), all test specimens demonstrated low moisture vapour resistance (Fig. 8a), in respect of the evaporative resistance rating (0–30) for acceptable clothing thermal comfort (Houshyar et al. 2015). This was attributed to the porosity of nonwoven fabrics and the excellent hydrophilicity of constituent viscose fibres. Among the specimens, control nonwoven fabrics had the least resistance against evaporative transmittance. The PAN nanofibrous membrane with low permeability due to less porosity (Fig. S3a) resisted moisture vapour transmission through the fabric, and therefore, PAN–nonwoven specimen (PF), demonstrated the maximum evaporative resistance. A slight increase in moisture transmittance was observed for the PAN–aerogel nonwoven fabrics because of increased porosity (Fig. S3b) of NF membranes after adding aerogel particles. Nevertheless, the evaporative resistance of all the test specimens (CF: 8.52; PF: 12.05; PAF1: 11.63; PAF2: 10.71 Pa m^2/W) is considered acceptable for thermal comfort, as the values lie within the evaporative performance rating range of 6–13 (highly

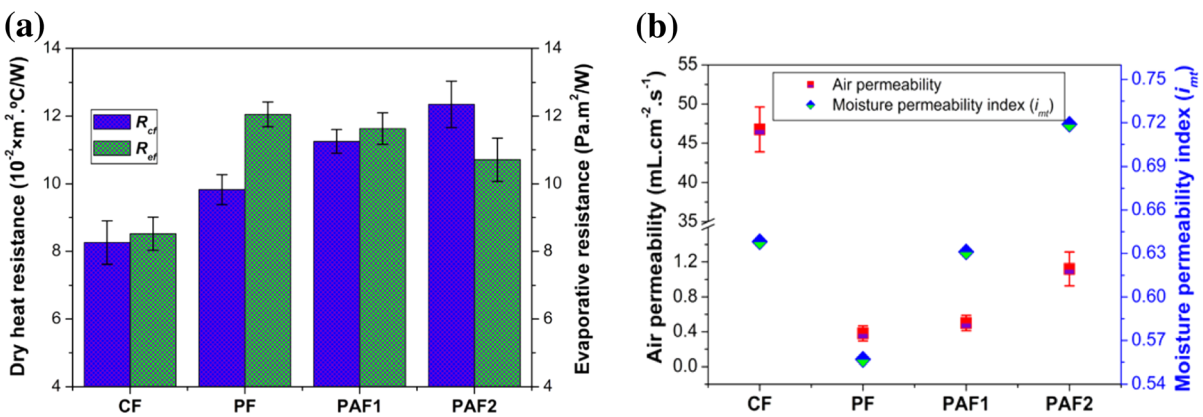

Fig. 8 Fabric thermal comfort. **a** thermal resistance (R_{cf}) and evaporative resistance (R_{ef}) **b** air permeability and moisture permeability index (i_{mt}). Data are represented as mean ± standard deviation (SD)

permeable with very good comfort at the medium activity rate) (Bhuiyan et al. 2020). The low evaporative resistance of the fabrics suggests that they are sufficiently breathable with adequate permeability to moisture vapour, and are expected to provide satisfactory thermal comfort for the wearer, working at a moderate, and to some extent at a higher activity rate.

The evaporative cooling index (i_{mt}) of the test specimens in Fig. 8b shows an enhanced permeability index of nonwoven specimens integrated with PAN–silica aerogel nanofibrous membrane. The minimum evaporative cooling index value of 0.557 was observed for the PAN–nonwoven fabric, whereas PAN–aerogel fabric with 4.0% aerogel (PAF2) had the maximum value (0.719). As the evaporative cooling index is the ratio of dry to evaporative heat resistance of the system, thus a higher proportion of the rise in thermal resistance compared with the evaporative resistance improved the overall permeability index of the PAN–aerogel nonwoven fabrics. The high moisture permeability index of PAF2 indicates that the fabrics can create satisfactory thermal comfort within the apparel–skin microenvironment in hot and humid conditions by shielding the body from atmospheric heat as well as readily transferring metabolic heat from the body to the atmosphere.

The air permeability regarding the breathability of the test nonwoven fabrics is shown in Fig. 8b. Among the fabrics, control specimens exhibited maximum breathability with an average value of 46.74 mL cm^{-2} s^{-1}. However, an abrupt reduction of permeability was observed for the fabrics integrated with nanofibrous membranes (Fig. 8b). Air permeability is directly related to fabric openness, i.e., the porousness or compactness of the cloth (Kothari and Newton 1974). Hence, a sharp reduction of fabric porosity due to the integration of less porous nanofibre membrane with the nonwoven fabric decreased the overall permeability of the fabric. An improved air permeability compared with the PAN–nonwoven fabric was found for the PAN–aerogel fabrics (Fig. 8b). The high porosity of the PAN–aerogel membrane contributed to this enhanced permeability. The air permeability also increased as the aerogel concentration increased.

Fabric air permeability is generally considered an important factor in estimating the clothing thermal comfort (Zupin et al. 2012) and therefore, it is used to determine the breathability of protective clothing employed for various special purposes (Saville 1999). Although the air permeability of nonwoven fabrics decreased apparently after its integration with the nanofibrous membrane, the average air permeability of the PAN–aerogel fabric (PAF1: 0.50 and PAF2: 1.12 mL cm^{-2} s^{-1}) is still considerably high compared with the breathability of several barrier clothing systems discussed in some recent studies (Bhuiyan et al. 2019c; Moiz et al. 2016, 2017). Moreover, the high moisture vapour transmittance and evaporative cooling index of the PAN–aerogel specimens endorsed the acceptable breathability of the fabric for thermal comfort. This permeability of PAN–aerogel fabrics can be utilised to facilitate the transfer of air and moisture vapour from the body to the environment and vice versa, providing acceptable thermal comfort with heat and chemical protection to the wearer.

Moisture management performance

The moisture management performance profiles of the nonwoven fabrics are shown in Fig. 9. Moisture management performance was assessed in terms of wetting time, absorption rate, spreading speed of liquid, one-way liquid transport capability (OWTC), and overall moisture management capacity (OMMC). The results are shown in Table 4. Among the fabrics, control nonwoven specimens exhibited an efficient moisture management performance, including minimum wetting time (4.96 s), maximum absorption rate (45.91%/s), and spreading (2.03 mm/s) of liquids to the fabric bottom surface. Thus, the fabric demonstrated the highest OWTC (19.69) and OMMC (0.169). This was due to the excellent hydrophilicity of viscose fibres along with a less compact structure of nonwoven fabrics, enabling an easy absorption, spreading, and penetration of aqueous solution through the fabric (Fig. S5).

A changed moisture management profile was noticed for the PAN–nonwoven fabric (PF), which transferred a small amount of liquids to the bottom surface (Fig. 9). The sandwiching of hydrophobic PAN nanofibrous membrane inside the fabric layers hindered the penetration and spreading of the aqueous solution from the inner to the outer surface; thus, the fabric demonstrated an excessive wetting time and low absorption rate with a negative OWTC (− 178.25) and a very low OMMC (0.096) (Table 4). PAN–silica aerogel nonwoven specimens exhibited the maximum

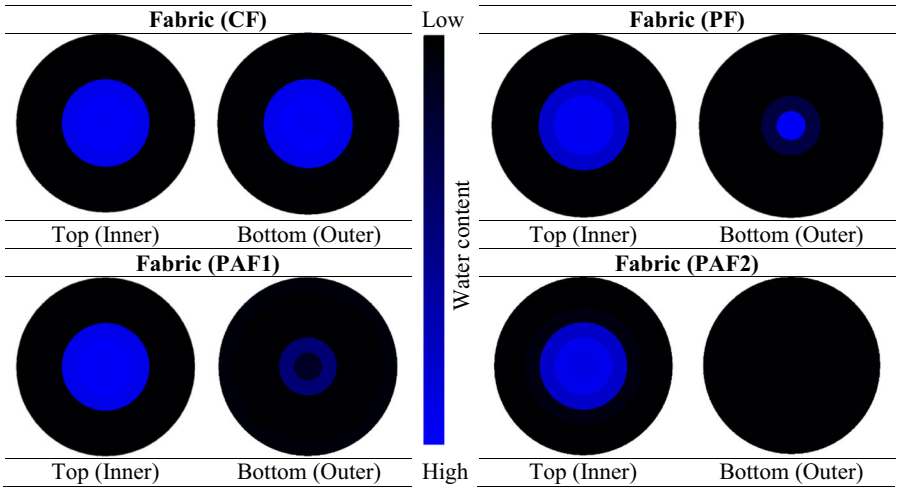

Fig. 9 Liquid transfer from the inner surface to the outer surface of fabrics after wetting 120 s

Table 4 Moisture management performance profile of test fabric specimens

Sample	Wetting time (s)		Absorption rate (%/s)		Spreading speed (mm/s)		OWTC	OMMC
	Top	Bottom	Top	Bottom	Top	Bottom		
CF	7.03	4.96	51.65	45.91	1.83	2.03	19.69	0.169
PF	7.31	9.18	41.39	35.90	1.73	0.53	− 178.25	0.096
PAF1	6.37	120	37.30	0.0	1.74	0.0	− 203.15	0.0
PAF2	6.18	120	29.48	0.0	1.55	0.0	− 397.51	0.0

OWTC one-way transport capability, *OMMC* overall moisture management capacity

wetting time (120 s) and zero absorption and spreading of liquids to the outer surface of the fabric, indicating the impermeable nature of the membrane to the water (Fig. S5). This impermeability of the PAN–silica aerogel membrane makes the barrier fabric impervious to liquids, keeping the wearer protected from toxic liquid chemicals.

Moisture management of textiles is commonly used to assess fabric thermal comfort, concerning wet clinginess, and this method quantitatively measures the absorption of liquid perspiration via the clothing in the apparel–skin microenvironment and transfer of the liquid to the atmosphere through and across the clothing (Shaid et al. 2018b). Although, PAN–aerogel nonwoven fabrics have a low moisture management profile, predicting an inadequate thermal comfort for clothing. However, a satisfactory moisture vapour transmittance (Fig. 8a) and air permeability (Fig. 8b), along with excellent water uptake and evaporation rate of viscose nonwoven fabrics (Bhuiyan et al. 2020), outweigh the low moisture management profile for acceptable thermal comfort of clothing in hot weather.

Conclusion

An electrospun nanofibrous membrane was successfully developed by integrating silica aerogel particles within a PAN solution. Protective clothing with simultaneous barrier performance and thermal comfort was fabricated by sandwiching PAN–silica aerogel NFs between viscose nonwoven layers. The morphological investigation explored randomly deposited aerogel particles that were well dispersed in the membrane to provide functional properties for versatile protection. The functionalised nanofibres embedded with nonwoven fabrics offered improved protection against liquid chemical penetration by retaining greater amounts of chemicals. Increased resistance against radiant heat confirmed the reliable performance of the fabric for thermal protection. Additionally, the soft, drapable, and lightweight PAN–silica aerogel nonwoven fabrics demonstrated adequate thermal resistance and evaporative transmittance as well as improved moisture permeability index for satisfactory thermophysiological wear comfort.

The high evaporative cooling index and sufficient breathability prevailed over the low moisture management profile of the fabric, suggesting the diffusion of perspiration vapour through the membrane for favourable thermal comfort in the apparel–skin microenvironment. The overall outcome of the research establishes that the fabrication of nonwoven–PAN–silica aerogel electrospun protective clothing is an innovative approach for developing lightweight drapable clothing with versatile protective performance and thermophysiological wear comfort for the user.

Acknowledgments The authors are grateful to Ms Shelley MacRae for her support with laboratory instruments.

Author contributions MARB contributed to conceptualization, methodology, formal analysis, investigation, writing original draft. LW contributed to supervision, experimental design, review and editing. RAS contributed to review and editing. ZAA and TS contributed to experimental investigation and data analysis. All authors discussed the results and contributed to the final manuscript.

Funding The author(s) disclosed no financial support for the research, authorship, and/or publication of this article. M. A. Rahman Bhuiyan is thankful to RMIT University, Australia for scholarship support towards his Ph.D. study.

References

Babar AA, Wang X, Iqbal N, Yu J, Ding B (2017) Tailoring differential moisture transfer performance of nonwoven/polyacrylonitrile–SiO_2 nanofiber composite membranes. Adv Mater Interfaces 4:1700062. https://doi.org/10.1002/admi.201700062

Barhoum A, Pal K, Rahier H, Uludag H, Kim IS, Bechelany M (2019) Nanofibers as new-generation materials: from spinning and nano-spinning fabrication techniques to emerging applications. Appl Mater Today 17:1–35. https://doi.org/10.1016/j.apmt.2019.06.015

Bhuiyan MR, Wang L, Shaid A, Shanks RA, Ding J (2019a) Advances and applications of chemical protective clothing system J Ind Text 49:97–138 https://doi.org/10.1177/1528083718779426

Bhuiyan MR, Wang L, Shaid A, Shanks RA, Ding J (2019b) Polyurethane-aerogel incorporated coating on cotton fabric for chemical protection. Prog Organ Coat 131:100–110. https://doi.org/10.1016/j.porgcoat.2019.01.041

Bhuiyan MR, Wang L, Shanks RA, Ding J (2019c) Polyurethane–superabsorbent polymer-coated cotton fabric for thermophysiological wear comfort. J Mater Sci 54:9267–9281. https://doi.org/10.1007/s10853-019-03495-8

Bhuiyan MR, Wang L, Shaid A, Jahan I, Shanks RA (2020) Silica aerogel-integrated nonwoven protective fabrics for chemical and thermal protection and thermophysiological wear comfort. J Mater Sci 55:2405–2418. https://doi.org/10.1007/s10853-019-04203-2

Dhineshbabu NR, Karunakaran G, Suriyaprabha R, Manivasakan P, Rajendran V (2014) Electrospun MgO/Nylon 6 hybrid nanofibers for protective clothing. Nano-Micro Lett 6:46–54. https://doi.org/10.5101/nml.v6i1.p46-54

Dorcheh AS, Abbasi M (2008) Silica aerogel; synthesis, properties and characterization. J Mater Process Technol 199:10–26. https://doi.org/10.1016/j.jmatprotec.2007.10.060

Frydrych I, Dziworska G, Bilska J (2002) Comparative analysis of the thermal insulation properties of fabrics made of natural and man-made cellulose fibres. Fibres Text East Eur 10:40–44

Gavrilenko O, Wang X (2019) Functionalized nanofibrous coating on cotton fabrics. Cellulose 26:4175–4190. https://doi.org/10.1007/s10570-019-02342-y

Ghaffari S, Yousefzadeh M, Mousazadegan F (2019) Investigation of thermal comfort in nanofibrous three-layer fabric for cold weather protective clothing. Polym Eng Sci 59:2032–2040. https://doi.org/10.1002/pen.25203

Gibson P, Schreuder-Gibson H, Rivin D (2001) Transport properties of porous membranes based on electrospun nanofibers. Colloids Surf A Physicochem Eng Asp 187:469–481. https://doi.org/10.1016/S0927-7757(01)00616-1

Heikkilä P, Sipilä A, Peltola M, Harlin A, Taipale A (2007) Electrospun PA-66 coating on textile surfaces Text Res J 77:864–870 https://doi.org/10.1177/0040517507078241

Höffele S, Russell SJ, Brook DB (2005) Light-weight nonwoven thermal protection fabrics containing nanostructured materials. Int Nonwovens J 14:10–16

Houshyar S, Padhye R, Troynikov O, Nayak R, Ranjan S (2015) Evaluation and improvement of thermo-physiological comfort properties of firefighters' protective clothing containing super absorbent materials. J Text Inst 106:1394–1402. https://doi.org/10.1080/00405000.2014.995930

Im JS, Kim MI, Lee Y-S (2008) Preparation of PAN-based electrospun nanofiber webs containing TiO_2 for photocatalytic degradation. Mater Lett 62:3652–3655. https://doi.org/10.1016/j.matlet.2008.04.019

Jahan I, Moiz A, Wang X (2019) Creating an interconnected PVA nanofibrous membrane on cotton fabrics by dip-coating of PDMS–TMS for versatile protection without. compromising comfort Cellulose 26:8179–8190. https://doi.org/10.1007/s10570-019-02667-8(012345

Ji L, Zhang X (2008) Ultrafine polyacrylonitrile/silica composite fibers via electrospinning. Mater Lett 62:2161–2164. https://doi.org/10.1016/j.matlet.2007.11.051

Jin L, Hong K, Yoon K (2013) Effect of aerogel on thermal protective performance of firefighter clothing. J Fiber Bioeng Inf 6:315–324. https://doi.org/10.3993/jfbi0920-1309

Kapridaki C, Maravelaki-Kalaitzaki P (2013) TiO_2–SiO_2–PDMS nano-composite hydrophobic coating with self-cleaning properties for marble protection. Prog Org Coat 76:400–410. https://doi.org/10.1016/j.porgcoat.2012.10.006

Kiil S (2015) Quantitative analysis of silica aerogel-based thermal insulation coatings. Prog Organ Coat 89:26–34. https://doi.org/10.1016/j.porgcoat.2015.07.019

Kothari VK, Newton A (1974) The air-permeability of non-woven fabrics. J Text Inst 65:525–531. https://doi.org/10.1080/00405007408630140

Lee S, Kay Obendorf S (2006) Developing protective textile materials as barriers to liquid penetration using melt-electrospinning. J Appl Polymer Sci 102:3430–3437. https://doi.org/10.1002/app.24258

Lee S, Obendorf SK (2007) Transport properties of layered fabric systems based on electrospun nanofibers. Fibers Polym 8:501–506. https://doi.org/10.1007/BF02875872

Li D, Wang Y, Xia Y (2003) Electrospinning of polymeric and ceramic nanofibers as uniaxially aligned arrays. Nano Lett 3:1167–1171. https://doi.org/10.1021/nl0344256

Mao N, Russell S, Pourdeyhimi B (2007) Characterisation, testing and modelling of nonwoven fabrics. In: Russell S (ed) Handbook of nonwovens. Woodhead, Cambridge, pp 401–514

Mao X, Si Y, Chen Y, Yang L, Zhao F, Ding B, Yu J (2012) Silica nanofibrous membranes with robust flexibility and thermal stability for high-efficiency fine particulate filtration. RSC Adv 2:12216–12223. https://doi.org/10.1039/C2RA22086E

Moiz A, Padhye R, Wang X (2017) Coating of TPU-PDMS-TMS on polycotton fabrics for versatile. protection Polymers 9:660. https://doi.org/10.3390/polym9120660

Moiz A, Vijayan A, Padhye R, Wang X (2016) Chemical and water protective surface on cotton fabric by pad-knife-pad coating of WPU-PDMS-TMS. Cellulose 23:3377–3388. https://doi.org/10.1007/s10570-016-1028-5

Mortan W, Hearle L (2008) Physical properties of textile fibers, 4th edn. Woodhead, Cambridge

Nie G, Li Z, Lu X, Lei J, Zhang C, Wang C (2013) Fabrication of polyacrylonitrile/CuS composite nanofibers and their recycled application in catalysis for dye degradation. Appl Surf Sci 284:595–600. https://doi.org/10.1016/j.apsusc.2013.07.139

Paul HL, Diller KR (2003) Comparison of thermal insulation performance of fibrous materials for the advanced space suit. J Biomech Eng 125:639–647. https://doi.org/10.1115/1.1611885

Sabetzadeh N, Bahrambeygi H, Rabbi A, Nasouri K (2012) Thermal conductivity of polyacrylonitrile nanofibre web in various nanofibre diameters and surface densities. Micro Nano Lett 7:662–666. https://doi.org/10.1049/mnl.2012.0375

Saville B (1999) Physical testing of textiles, 1st edn. Woodhead, Cambridge

Scaffaro R, Lopresti F (2018) Properties-morphology relationships in electrospun mats based on polylactic acid and graphene nanoplatelets. Compos A Appl Sci Manuf 108:23–29. https://doi.org/10.1016/j.compositesa.2018.02.026

Shaid A, Wang L, Padhye R (2016) The thermal protection and comfort properties of aerogel and PCM-coated fabric for firefighter garment. J Ind Text 45:611–625 https://doi.org/10.1177/1528083715610296

Shaid A, Wang L, Fergusson SM, Padhye R (2018a) Effect of aerogel incorporation in PCM-containing thermal liner of firefighting garment. Cloth Text Res J 36:151–164 https://doi.org/10.1177/0887302X18755464

Shaid A, Wang L, Padhye R, Bhuyian MR (2018b) Aerogel nonwoven as reinforcement and batting material for firefighter's protective clothing: a comparative study. J Sol-Gel Sci Technol 87:95–104. https://doi.org/10.1007/s10971-018-4689-8

Shaid A, Wang L, Padhye R, Gregory M (2019) Low cost bench scale apparatus for measuring the thermal resistance of multilayered textile fabric against radiative and contact heat transfer. HardwareX. https://doi.org/10.1016/j.ohx.2019.e00060

Venkataraman M, Mishra R, Wiener J, Militky J, Kotresh T, Vaclavik M (2015) Novel techniques to analyse thermal performance of aerogel-treated blankets under extreme temperatures. J Text Inst 106:736–747. https://doi.org/10.1080/00405000.2014.939808

Venkataraman M, Mishra R, Militky J, Xiong X, Marek J, Yao J, Zhu G (2018) Electrospun nanofibrous membranes embedded with aerogel for advanced thermal and transport properties. Polym Advan Technol 29:2583–2592. https://doi.org/10.1002/pat.4369

Wang N, Si Y, Wang N, Sun G, El-Newehy M, Al-Deyab SS, Ding B (2014) Multilevel structured polyacrylonitrile/silica nanofibrous membranes for high-performance air filtration. Sep Purif Technol 126:44–51. https://doi.org/10.1016/j.seppur.2014.02.017

Wilson A (2007) Development of the nonwovens industry. In: Russell SJ (ed) Handbook of nonwovens. Woodhead, Cambridge, pp 1–15

Woodcock AH (1962) Moisture transfer in textile systems, part I. Text Res J 32:628–633 https://doi.org/10.1177/004051756203200802

Wu M, Wang Q, Li K, Wu Y, Liu H (2012) Optimization of stabilization conditions for electrospun polyacrylonitrile nanofibers. Polym Degrad Stab 97:1511–1519. https://doi.org/10.1016/j.polymdegradstab.2012.05.001

Xiong X, Yang T, Mishra R, Kanai H, Militky J (2018) Thermal and compression characteristics of aerogel-encapsulated textiles J Ind Text 47:1998–2013 https://doi.org/10.1177/1528083717716167

Yanilmaz M, Dirican M, Zhang X (2014) Evaluation of electrospun SiO2/nylon 6, 6 nanofiber membranes as a thermally-stable separator for lithium-ion batteries. Electrochim Acta 133:501–508. https://doi.org/10.1016/j.electacta.2014.04.109

Zhang W, Wang Y, Sun C (2007) Characterization on oxidative stabilization of polyacrylonitrile nanofibers prepared by electrospinning. J Polym Res 14:467–474. https://doi.org/10.1007/s10965-007-9130-x

Zupin Ž, Hladnik A, Dimitrovski K (2012) Prediction of one-layer woven fabrics air permeability using porosity parameters. Text Res J 82:117–128